

Magnetic order in YbMnO₃ studied by neutron diffraction and Mössbauer spectroscopyX. Fabréges,¹ I. Mirebeau,¹ P. Bonville,² S. Petit,¹ G. Lebras-Jasmin,² A. Forget,² G. André,¹ and S. Pailhès¹¹Laboratoire Léon Brillouin, CE-Saclay, CEA-CNRS, 91191 Gif-Sur-Yvette, France²DSM/Service de Physique de l'Etat Condensé, CE-Saclay, CEA-CNRS, 91191 Gif-Sur-Yvette, France

(Received 22 July 2008; revised manuscript received 30 September 2008; published 16 December 2008)

The magnetic ordering of the hexagonal multiferroic compound YbMnO₃ has been studied between 100 and 1.5 K by combining neutron powder diffraction, ¹⁷⁰Yb Mössbauer spectroscopy, and magnetization measurements. The Yb moments of the two crystallographic sites order at two different temperatures: the 4*b* site together with the Mn moments (at $T_N \approx 85$ K) and the 2*a* site well below (at 3.5 K). The temperature dependences of the Mn and Yb moments are explained within a molecular-field model, showing that the 4*b* and 2*a* sites order via Yb-Mn and Yb-Yb interactions, respectively. A simple picture taking into account the local Mn environment of the rare-earth *R* (4*b*) ion is proposed to couple *R* and Mn orders in hexagonal RMnO₃ manganites. The nature and symmetry of the *R*-Mn interactions yielding the *R* order are discussed.

DOI: [10.1103/PhysRevB.78.214422](https://doi.org/10.1103/PhysRevB.78.214422)

PACS number(s): 75.25.+z, 76.80.+y, 75.80.+q, 75.30.Kz

I. INTRODUCTION

RMnO₃ manganites, where the R^{3+} ions are either Y or a rare earth, belong to the multiferroic family, showing a coupling between magnetic and electric order parameters. This magnetoelectric (ME) coupling opens the possibility of tuning the magnetization by an electric field or vice versa, with potential application for building new kinds of electronic devices.^{1,2} Numerous experiments in the RMnO₃ series probe the key role of their noncollinear magnetic structures, induced by frustrated magnetic interactions, in driving such ME coupling.³ The ME coupling is also connected with a spin-lattice coupling recently observed in both structural⁴ and dynamical⁵⁻⁷ properties. Understanding the microscopic characteristics of the magnetic order and the origin of the magnetic interactions is a key issue for tuning their properties.

The RMnO₃ compounds are divided in two classes according to the ionic radius of the rare earth. Orthorhombic structures are stabilized for large ionic radius of the R^{3+} ion ($R = \text{La to Dy}$), whereas hexagonal structures are stable at small ionic radius ($R = \text{Y and Ho to Lu}$). In orthorhombic compounds where magnetic frustration arises from competing exchange interactions, ferroelectric and magnetic orders appear at the same temperature (~ 60 K), which suggests a strong ME coupling.⁸ In hexagonal compounds, magnetic frustration arises from the lattice geometry since the triangular Mn lattice is frustrated for antiferromagnetic (AF) first-neighbor interactions. Here, the ferroelectric order occurs around 900 K, well above the magnetic ordering temperature (~ 80 K). The ME coupling is evidenced for instance by anomalies in the dielectric constant⁹ or specific heat¹⁰ at the magnetic transitions.

In spite of numerous experiments, the complex magnetic structures of the RMnO₃ are still not fully understood. This is especially true for the hexagonal compounds, where homometric configurations of the Mn moments in the triangular Mn lattice are extremely difficult to distinguish, and where the *R* magnetic order is intricate, owing to the presence of two different crystallographic rare-earth sites.¹¹

Here we present a detailed study of the magnetic order in YbMnO₃ using neutron diffraction, Mössbauer spectroscopy

on the isotope ¹⁷⁰Yb, and magnetization measurements. The magnetic structure of this compound has not been studied up to now, although precise predictions could be made from optical spectroscopy data.¹² By combining microscopic and macroscopic probes in a large temperature range ($1.5 < T < 100$ K), we provide a complete determination of the magnetic structure.

The *T* dependence of the Mn and Yb moments derived from our experiments can be explained quantitatively within the molecular-field model. This allows us to clarify the respective roles of Mn-Mn, *R*-Mn, and *R*-*R* interactions in this compound. Using these results, we discuss the symmetry and the possible origins of the magnetic *R*-Mn interactions, and we propose a simple picture, which may hold for the whole hexagonal family.

II. EXPERIMENTAL DETAILS

A polycrystalline sample of YbMnO₃ was prepared as described in Ref. 13 and characterized using x-ray diffraction at room temperature, showing that the sample is single phased. Magnetic measurements were performed with a superconducting quantum interference device (SQUID) magnetometer between 1.5 and 300 K.

Mössbauer spectroscopy on ¹⁷⁰Yb realizes γ -ray resonant absorption between the ground nuclear state, with spin $I_g = 0$, and the first-excited state, with spin $I_e = 2$, at an energy of 84.3 keV. We used a neutron-activated Tm^{*}B₁₂ γ -ray source mounted on a triangular velocity electromagnetic drive. ¹⁷⁰Yb Mössbauer absorption spectra were recorded in the temperature range of 1.35–50 K.

The crystal structure was determined by measuring a neutron powder-diffraction (NPD) pattern at 300 K on the high-resolution powder diffractometer 3T2 of the Laboratoire Léon Brillouin (LLB) at Orphée reactor, with an incident neutron wavelength $\lambda = 1.2253$ Å. The magnetic structure was studied by collecting NPD patterns at several temperatures, between 100 K (above the magnetic transition) and 1.5 K, on the neutron diffractometer G4-1 of the LLB, with an incident neutron wavelength of 2.4226 Å. Both crystal and magnetic structures were refined using the FULLPROF suite.¹⁴

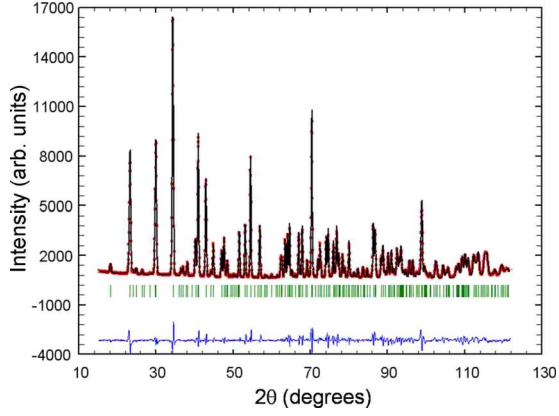


FIG. 1. (Color online) Observed and FULLPROF calculated NPD pattern at room temperature. The Bragg reflections (ticks) and the difference between the observed and calculated patterns are plotted at the bottom.

III. CRYSTAL STRUCTURE

The refined NPD pattern at 300 K is shown in Fig. 1. All Bragg reflections of the pattern can be indexed within the hexagonal space group $P6_3cm$. The lattice constants at 300 K are $a=6.0629(1)$ Å and $c=11.3529(1)$ Å.

The refined atomic positions are reported in Table I. They are in good agreement with previous determinations from x-ray diffraction.^{15,16} As already stated in Ref. 17, the lattice unit cell consists of 6 f.u. Each Mn atom is surrounded by oxygen ions forming a MnO_5 bipyramidal structure, with three O (two O_4 and one O_3) ions close to the Mn plane and two O (O_1 and O_2) ions at the apexes. Corner sharing MnO_5 bipyramids form layers separated along the c axis by Yb layers. In the space group $P6_3cm$, Yb occupies the two crystallographically inequivalent sites $2a$ and $4b$, with trigonal local symmetry around the hexagonal c axis. The Yb($4b$) site consists of four equivalent atomic positions inside the hexagonal unit cell and the Yb($2a$) site of two equivalent atomic positions along the c -axis edges of the cell.

IV. MAGNETIC SUSCEPTIBILITY AND ^{170}Yb MÖSSBAUER DATA

The thermal variation in the magnetic susceptibility $\chi(T)$, measured in a field of 20 G, is shown in Fig. 2. The inverse

TABLE I. Atom positions and discrepancy factors at room temperature.

| Atoms | x | y | z |
|---------------------|---------------|---------------|----------|
| Yb($2a$) | 0 | 0 | 0.274(2) |
| Yb($4b$) | $\frac{1}{3}$ | $\frac{2}{3}$ | 0.232(2) |
| Mn($6c$) | 0.345(4) | 0 | 0 |
| O_1 ($6c$) | 0.307(2) | 0 | 0.165(3) |
| O_2 ($6c$) | 0.640(1) | 0 | 0.336(3) |
| O_3 ($4b$) | 0 | 0 | 0.475(2) |
| O_4 ($2a$) | $\frac{1}{3}$ | $\frac{2}{3}$ | 0.020(2) |
| Bragg R factor | | 4.32% | |
| Discrepancy factors | RF factor | 3.21% | |

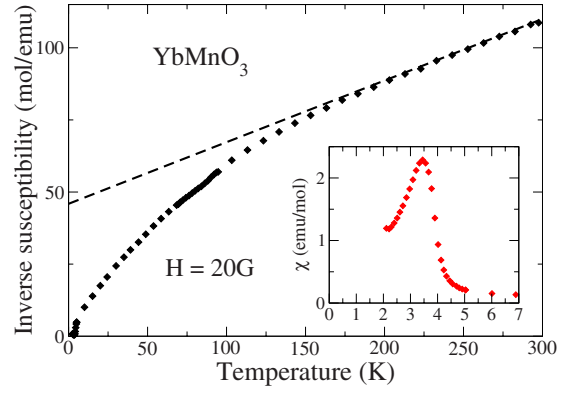


FIG. 2. (Color online) Inverse magnetic susceptibility in YbMnO_3 . The dashed line is a Curie-Weiss law with $\mu_{\text{eff}}=6.1\mu_B$ and $\theta_p=-220$ K. Inset: low-temperature susceptibility.

susceptibility follows a Curie-Weiss law in the temperature range of 200–300 K, with an effective moment $\mu_{\text{eff}}=6.1(1)\mu_B$ and a paramagnetic Curie temperature $\theta_p \approx -220(5)$ K (antiferromagnetic). As will be shown in Sec. V, the Néel temperature in YbMnO_3 is $T_N \approx 85$ K. The large negative θ_p value, such that $|\theta_p|/T_N \approx 2.5$, could be linked to the frustration of the Mn moments on their triangular lattice. Assuming for Yb^{3+} the free ion value $\mu_{\text{eff}}=4.54\mu_B$, we obtain an effective moment of $4.1(1)\mu_B$ for the Mn^{3+} ion ($S=2$), which is lower than the value of $4.9\mu_B$ expected for $g=2$. This deviation could be due to our limited experimental temperature range where the Curie-Weiss law holds; indeed, susceptibility measurements performed in a single crystal up to 350 K (Ref. 18) obtain the correct effective moment with the free ion values for both ions. No anomaly in $\chi(T)$ is found at the magnetic transition, in contrast to magnetic measurements in single crystals,^{10,18} where $\chi_c(T)$ exhibits a small peak at T_N . At low temperature, a ferromagnetic-like increase in $\chi(T)$ occurs at 3.5 K (inset of Fig. 2). This behavior is consistent with the hysteresis and the step increase in the high field magnetization reported in single crystals measurements below 3 K.¹⁹ We interpret it by the onset of magnetic ordering among the Yb($2a$) ions, as confirmed by the Mössbauer data to be described next.

The ^{170}Yb Mössbauer spectra at selected temperatures are shown in Fig. 3. Between 1.35 and 25 K, they show two subspectra with relative weights close to the ratio 1:2, which we attribute, respectively, to Yb($2a$) and Yb($4b$) sites. Above 25 K, the spectra are no longer resolved and consist of a single line. In Fig. 3, the Yb($2a$) subspectrum corresponds to the red line and the Yb($4b$) to the blue line. At 1.35 K, both subspectra are five-line magnetic hyperfine patterns, with a small quadrupolar hyperfine interaction. The weakness of the latter precludes any reliable information about the orientation of the hyperfine field with respect to the c axis to be obtained. The hyperfine fields are, respectively, 117(3) and 180(3) T for site Yb($2a$) and Yb($4b$). Using the proportionality constant $C=102$ T/ μ_B linking the hyperfine field and the Yb^{3+} magnetic moment,²⁰ the saturated moment is $1.15(3)\mu_B$ for Yb($2a$) and $1.76(3)\mu_B$ for Yb($4b$).

As temperature increases, the Yb($2a$) hyperfine field, and thus the moment, slowly decreases down to 3 K, reaching

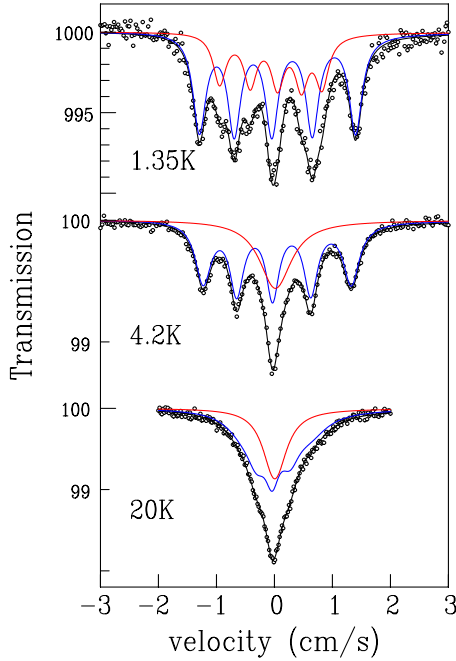


FIG. 3. (Color online) ^{170}Yb Mössbauer spectra in YbMnO_3 at selected temperatures. The subspectrum corresponding to the minority $\text{Yb}(2a)$ site (relative occupancy 1/3) is drawn in red and that corresponding to the $\text{Yb}(4b)$ site in blue.

$1.00(3)\mu_B$ at 3 K. A spectral change occurs between 3 and 3.5 K on the $\text{Yb}(2a)$ subspectrum. The hyperfine field pattern transforms into a single unresolved broad line at 3.5 K (see the red subspectrum at 4.2 K in Fig. 3). Therefore, the hyperfine field vanishes on this site above 3.5 K, and the $\text{Yb}(2a)$ ion becomes paramagnetic. The Mössbauer line shape then reflects the ionic fluctuations within the ground Kramers doublet and its interpretation is postponed until the end of this section. The ordering of the $\text{Yb}(2a)$ moments below 3.5 K is also observed on the magnetic susceptibility, which shows a large ferromagneticlike anomaly at the transition (see inset of Fig. 2). The $\text{Yb}(4b)$ subspectrum shows no qualitative change from 1.35 to 25 K. The hyperfine field decreases, reaching $59(5)$ T [i.e., a moment of $0.58(5)\mu_B$] at 25 K. At higher temperature, it is not possible to distinguish the $\text{Yb}(2a)$ and $\text{Yb}(4b)$ subspectra. The thermal variation in the $\text{Yb}(4b)$ moment is presented in Sec. VI in comparison with the moment values derived from neutron diffraction. Our 4.2 K spectrum is in agreement with that of a recent ^{57}Fe and ^{170}Yb Mössbauer study.²¹

The behaviors of the Yb ions at the two sites are thus rather different. Above 3.5 K, there is a vanishing molecular field at the $2a$ site, which means that the exchange field from the Mn ions is zero. This is not the case for the Yb ions at the $4a$ sites, which are polarized by Mn exchange up to at least 20 K. The neutron study described below shows that this exchange field is present up to 40 K, and probably up to T_N . This behavior is similar to that in HoMnO_3 .

The paramagnetic relaxation of the $\text{Yb}(2a)$ ion can be interpreted using the Mössbauer relaxational line shape developed in Ref. 22. Since the $\text{Yb}(2a)$ subspectrum consists of a single line, the “extreme narrowing” regime holds for the

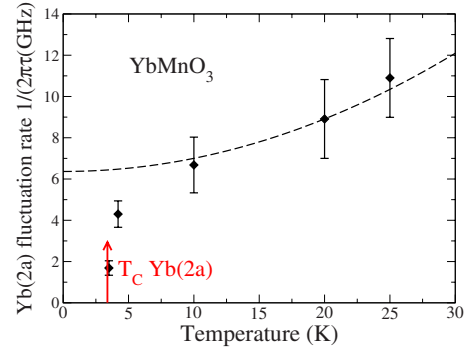


FIG. 4. (Color online) Thermal variation in the $\text{Yb}^{3+}(2a)$ relaxation rate extracted from the ^{170}Yb Mössbauer spectra in YbMnO_3 . The dashed line is a guide for the eyes and the red arrow marks the (probably) ferromagnetic transition of the $\text{Yb}(2a)$ sites.

fluctuation rate of $1/2\pi\tau$, i.e., $\hbar/\tau \gg A$, where A is the hyperfine constant associated with the Yb^{3+} ground Kramers doublet and the excited nuclear state of the ^{170}Yb isotope. It is related to the above-mentioned proportionality constant C by²³ $A = Cg\mu_B g_n \mu_n$, where g and g_n are, respectively, the electronic and nuclear gyromagnetic ratios (or g factors) and μ_n is the nuclear Bohr magneton. Using the $\text{Yb}(2a)$ saturated moment value of $1.15\mu_B$, yielding $g=2.3$, one gets $A = 580$ MHz. Since the width of the $\text{Yb}(2a)$ line narrows as temperature increases, the spin-relaxation rate increases according to the expression for the dynamical broadening²² $\Delta\Gamma_R = 3A^2\tau$. The fitted values of the relaxation rate of $1/2\pi\tau$ are represented in Fig. 4. It slows down abruptly when approaching the transition near 3.5 K from above (“critical slowing down”); the $T=0$ “extrapolated” value of ≈ 6 GHz is due to exchange-driven spin-spin relaxation and the increase above 10 K can be caused by phonon-driven relaxation.

V. MAGNETIC STRUCTURE

The thermal evolution of the NPD patterns is shown in Fig. 5. The temperature dependences of the integrated intensities of typical Bragg peaks (100), (101), and (102) are shown in Fig. 6. Strong changes occur around $T_N=86$ K, which corresponds to the magnetic transition. Below this temperature, an intensity of magnetic origin grows at the (100) and (101) Bragg positions, where the nuclear reflections are forbidden by the $P6_3cm$ symmetry, and the intensity of the (102) peak strongly increases due to an additional magnetic contribution. All peaks can be indexed within the hexagonal space group $P6_3cm$ and a propagation vector $\vec{k} = 0$; this points to an AF structure having the same unit cell as the chemical one since a ferromagnetic (F) ordering can be excluded from the absence of anomaly in the susceptibility at the transition.

The temperature dependences of the (100) and (101) Bragg peaks strongly differ from each other. The (100) peak remains rather weak down to about 20 K then suddenly increases below. In contrast, the (101) peak increases abruptly below 86 K. These variations suggest that the (100) and

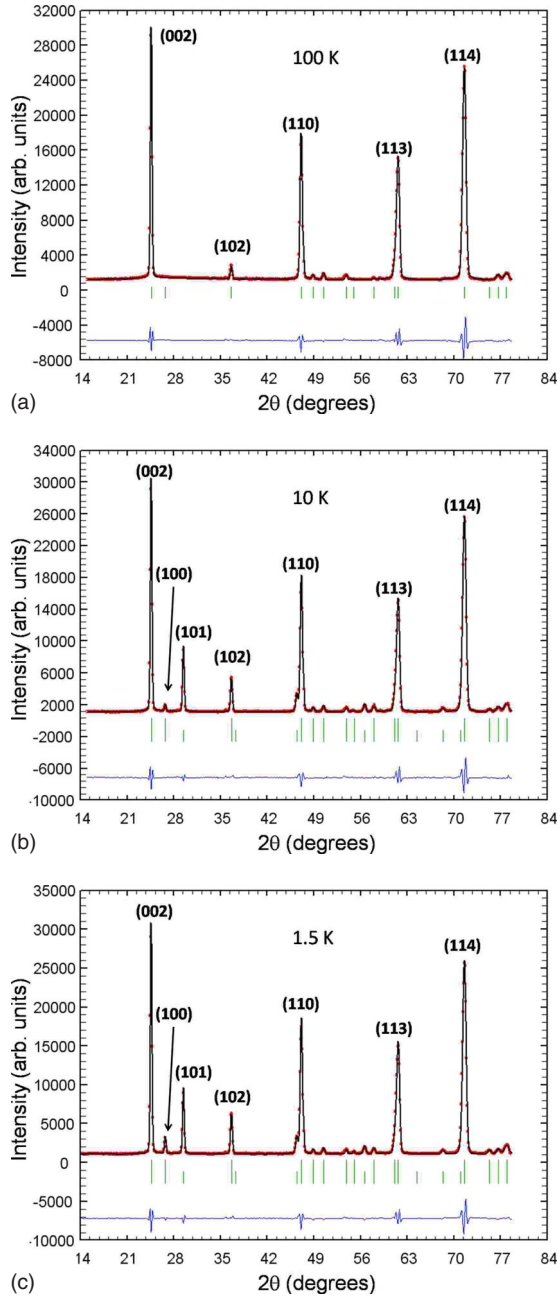


FIG. 5. (Color online) Observed and FULLPROF calculated NPD patterns between 1.5 and 100 K. The Bragg reflections (ticks) and the difference between the observed and calculated patterns are plotted at the bottom.

(101) peak intensities are controlled by Yb and Mn ordering, respectively, with the (102) Bragg peak involving contributions of both orderings. Moreover, one observes a strong (101) peak in YbMnO₃, with thermal evolution akin to that of the (100) peak in YMnO₃.¹⁷ Recalling that, in YMnO₃, the Mn order does not induce a strong (101) magnetic peak, it means that Mn order is affected by Y/Yb substitution. Finally, the temperature dependence of all magnetic peaks is monotonic, in contrast to HoMnO₃ where Mn magnetic moments reorient at low temperature.

A. Mn order

To analyze the magnetic structure we searched for all irreducible representations (IRs) compatible with the crystal symmetry using the theory of group representation analysis²⁴ and the program BASIREPS.²⁵ Description of this analysis for hexagonal RMnO₃ compounds was already given in Ref. 17. The atomic positions in the unit cell were kept fixed and equal to those determined above. In the space group $P6_3cm$ with $\vec{k}=0$ propagation vector, one finds six IRs, corresponding to the six possible configurations of the Mn moments reported in Fig. 7. In these configurations, the Mn moments lie in the ab plane and their vectorial sum is zero. This results from the frustration of the Mn moments in their triangular lattice.

It is important to notice that the Γ_2 and the Γ_4 configurations are homometric (namely, cannot be distinguished by NPD) as well as Γ_1 and Γ_3 .²⁶ The best fit of the data was obtained assuming Mn ordering which corresponds to the irreducible representation Γ_2 or Γ_4 , in contrast to YMnO₃ where it corresponds to a Γ_1 or Γ_3 IR. The saturated Mn moment value is $3.25\mu_B$, which is lower than the value of $4\mu_B$ expected for $g=2$ and $S=2$.

B. Yb order

The magnetic order of Yb moments is more intricate and difficult to determine unambiguously using neutron diffraction only since the two crystallographic $2a$ and $4b$ sites order independently. Space-group symmetry allows two types of magnetic orders: along the c axis or in the ab plane, and the coupling between the Yb ions can be antiferromagnetic or F, leading to six possibilities. The Mössbauer spectroscopy data show that the low-temperature Yb magnetic moments are small: $1.76\mu_B$ for Yb($4b$) and $1.15\mu_B$ for Yb($2a$), as compared to the saturated Mn moment value of $3.25\mu_B$. Then the magnetic ordering of the Yb sublattices only gives incremental contributions to the NPD spectra, and their magnetic structure was solved with the help of Mössbauer spectroscopy.

In the temperature range $3.5 < T < 86$ K, we considered contributions only from ordered magnetic moments on the Yb($4b$) sites. For $T < 3.5$ K, we considered also ordered moments on the Yb($2a$) sites. As to the $4b$ sites, the best agreement with the NPD patterns is obtained for Yb moments oriented along the c axis. We find that the Yb moments of the $4b$ sites are antiferromagnetically coupled within a given layer, and that the z and $z + \frac{1}{2}$ layers are ferromagnetically coupled. At $T=3.7$ K, this refinement yields a discrepancy factor R_{Mag} of about 3.1%, which is much better than the values around 20% given by alternative solutions. As shown in Fig. 8, the moment values on the Yb($4b$) sites deduced from NPD patterns are in excellent agreement with those obtained from the Mössbauer spectra.

As to the $2a$ sites, which order below 3.5 K with much smaller moments, we fixed the moments to the values deduced from the Mössbauer spectra. The orientation of the moments was refined using our NPD data. There are two possibilities for the Yb($2a$) to orient: along the c axis or in the ab plane. Taking into account the ferromagneticlike in-

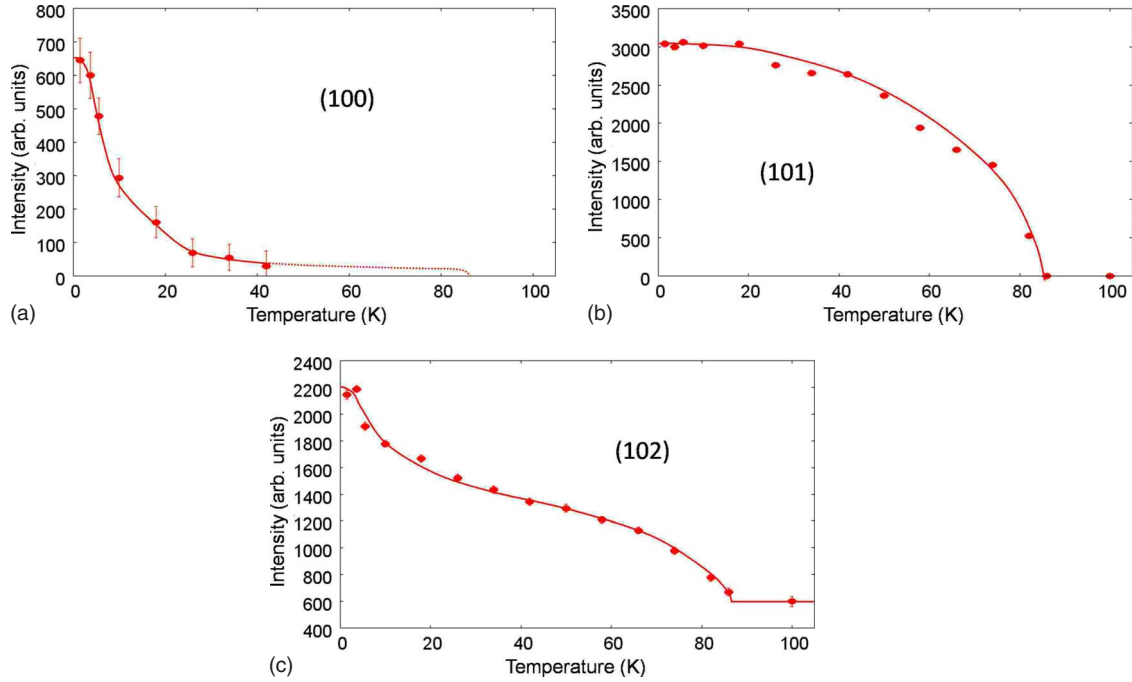


FIG. 6. (Color online) Integrated intensities of the (100), (101), and (102) reflections between 1.5 and 100 K (lines are guides for the eyes).

crease in the susceptibility at 3.5 K, we assume an F coupling between two adjacent Yb(2a) layers. We obtain a discrepancy factor of $R=3.05\%$ for the 2a moments in the ab plane, which is slightly better than for the moments along the c axis ($R=3.44\%$). It suggests that the Yb(2a) moments lie in the ab plane. In applied field, the reorientation of the ferromagnetic Yb(2a) moments from the ab plane to the c axis could thus explain the steplike increase of the magnetization observed for $H\parallel c$ in Ref. 19. This increase, of about $1.5\mu_B/\text{f.u.}$ at 1.8 K, is in good agreement with the Yb(2a) moment value ($1.13\mu_B$) found here.

Finally, the moment values at 1.5 K are $m_{\text{Mn}}=3.23(5)\mu_B$, $m_{\text{Yb}(4b)}=1.77(5)\mu_B$, and $m_{\text{Yb}(2a)}=1.13(5)\mu_B$. The evolution

of the moments versus temperature is plotted in Fig. 8.

VI. DISCUSSION

In YbMnO₃, the Mn magnetic order with Γ_2 or Γ_4 symmetry agrees with expectations from optical measurements.¹² Such a type of order is also expected from the general tendency observed in hexagonal RMnO₃ compounds versus the rare-earth ionic radius.²⁷ $\Gamma_{2,4}$ magnetic orders seem to be stabilized for low ionic radius (Er, Yb, and Lu) and $\Gamma_{1,3}$ for higher ionic radius (Ho, Y, and Y-Er). This could be related to the amplitude of the distortion of the Mn lattice with respect to triangular symmetry.

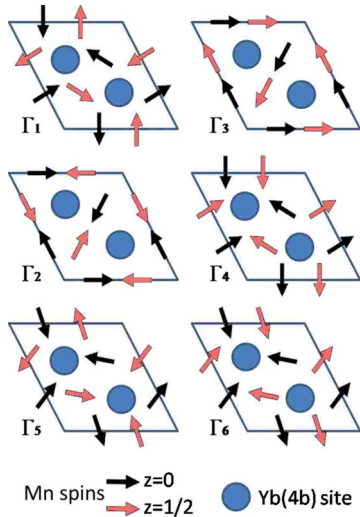


FIG. 7. (Color online) Symmetry allowed Mn spin orders in hexagonal RMnO₃. In YbMnO₃, Γ_2 or Γ_4 IR yield the best fit to experiment.

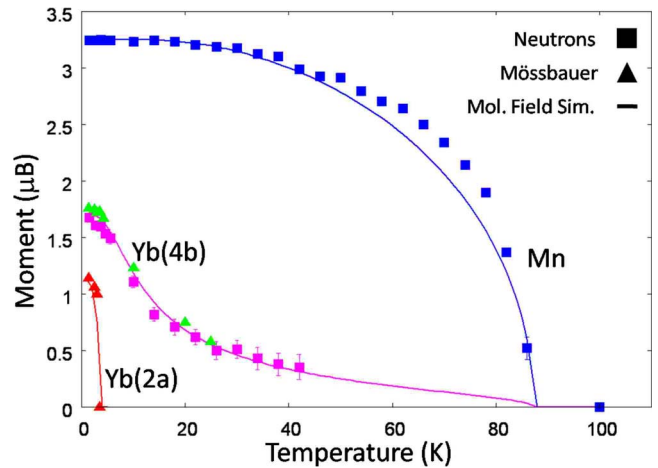


FIG. 8. (Color online) Observed Mn, Yb(4b), and Yb(2a) moments from NPD and Mössbauer measurements (dots) versus temperature. The solid lines correspond to the molecular-field calculation.

As concerns the rare-earth moments, we found that the $4b$ and $2a$ sites order independently. This is also the case in HoMnO_3 , where ordered Ho moments on $4b$ sites are observed below 35–40 K, whereas Ho $2a$ sites remain paramagnetic down to 5 K.²⁸ In HoMnO_3 , a change in the Mn structure (from $\Gamma_{2,4}$ above 38 K to $\Gamma_{1,3}$ below) occurs together with the rare-earth ordering. This is not the case for YbMnO_3 , possibly due to the lower value of the Yb moment.

In spite of a very large amount of experimental and theoretical works, the nature of the interactions which control the magnetic structure in RMnO_3 compounds is still unclear.^{28,29} To shed some light on this point, we first compare the measured temperature dependence of Mn and Yb moments with calculations from a molecular-field model. Then we briefly discuss the symmetry of interactions necessary to explain the observed magnetic orders. Finally, we propose possible origins for the magnetic interactions in RMnO_3 that are compatible with both experiment and calculations.

A. Molecular-field analysis

The thermal variations in the Mn and Yb magnetic moments derived from both neutron and Mössbauer data are shown in Fig. 8. The Yb($4b$) moment values derived from both techniques are in remarkable agreement, and their thermal variation has an unusual shape, with an upward curvature in a large temperature range. We applied the molecular-field model in order to calculate these thermal variations. We first obtained the T dependence of the Mn moment by a self-consistent mean-field calculation using the Brillouin function $B_2(x)$ for $S=2$ and a molecular-field constant λ_0 representing Mn-Mn exchange. The standard formula has to be slightly modified because the saturated Mn moment of $m_{\text{sat}}=3.23(5)\mu_B$ is lower than $gS\mu_B=4\mu_B$. So we used the following expression:

$$m_{\text{Mn}}(T) = m_{\text{sat}} B_2 \left[\frac{g\mu_B S \lambda_0 m_{\text{Mn}}(T)}{k_B T} \right], \quad (1)$$

which ensures that saturation occurs at $m_{\text{sat}}=3.3\mu_B$. We obtain a good fit of the experimental data (blue line in Fig. 8) with $\lambda_0=19 \text{ T}/\mu_B$. Then we fitted the T dependence of the Yb($4b$) moment assuming that the ground crystal-field doublet alone is populated, i.e., describing the Yb ion by an effective spin $S=1/2$, with a g factor g_{Yb} in the direction of the net exchange field from the Mn ions. Since the saturated Yb($4b$) moment is $m_0=\frac{1}{2}g_{\text{Yb}}\mu_B=1.75\mu_B$, then $g_{\text{Yb}}=3.5$. The Yb($4b$) ion is submitted to a molecular field $\lambda_1 m_{\text{Mn}}$ from Yb-Mn exchange since we neglect Yb-Yb exchange. Its moment is then calculated using the expression

$$m_{\text{Yb}}(T) = \frac{1}{2} g_{\text{Yb}} \mu_B \tanh \left[\frac{g_{\text{Yb}} \mu_B \lambda_1 m_{\text{Mn}}(T)}{2k_B T} \right], \quad (2)$$

where $m_{\text{Mn}}(T)$ is obtained from expression (1). We obtain a good fit to the data (magenta line in Fig. 8) with $\lambda_1=2.1 \text{ T}/\mu_B$. The unusual upward curvature comes from the tanh function with a small argument, with the constant λ_1 being much smaller than λ_0 . With this model, a small ordered Yb moment should persist up to $T_N=86 \text{ K}$, with a value

below $0.3\mu_B$, which is beyond the accuracy of neutron and Mössbauer probes. We conclude that the Yb ions on the $4b$ sites orient in a nonvanishing net molecular field through Yb-Mn exchange. As to the Yb moment on the $2a$ sites, their much lower ordering temperature (3.5 K) strongly suggests that they orient in their own molecular field through Yb-Yb interactions. From this analysis follows the hierarchy of exchange interactions in YbMnO_3 , in decreasing order: Mn-Mn, Yb-Mn, and Yb-Yb. Similar conclusions could be valid for other R ions (Ho and Er) in hexagonal RMnO_3 .

B. Mn environment of a R ion

Assuming that $R(4b)$ moments order via R -Mn interactions, we consider the Mn environment around a $R(4b)$ site, taking into account nearest-neighbor Mn ions only. In the following we will consider only the first four IRs (Γ_1 – Γ_4) which describe the magnetism of the whole RMnO_3 family (see Fig. 5). The moment on a $R(4b)$ site is expected to orient along the c axis to obey the trigonal symmetry of its Mn environment. This agrees with our observations in YbMnO_3 and with the magnetic order in HoMnO_3 .^{30,31}

In order to depict the local magnetic environment of each $R(4b)$ site, we need to take into account the orientation and position of the Mn moments. For this purpose, we define the A factors as

$$A_i = \sum_j \vec{S}_j \cdot \vec{r}_{ij}, \quad (3)$$

where the sum runs over the three Mn first neighbors of the $R(4b)$ site in a particular plane, \vec{S}_j is the magnetic moment of Mn at site j , and \vec{r}_{ij} is the vector joining Mn site j to $R(4b)$ site i .

The A factors are either positive (+) or negative (–) for a given Mn plane depending on the magnetic configuration Γ_i of the Mn ions. This leads to four possible magnetic environments for the $R(4b)$ ion, (++) , (––) , (+–) , and (–+), defined by the signs of the ($A_i^{\text{up}} A_i^{\text{down}}$) pairs associated with upper and lower Mn planes. One can easily see that there are either only one or two opposite A pairs allowed for each IR, whatever the IR retained for the Mn order. Considering that R moments in environments with identical (opposite) A pairs align parallel (antiparallel) along c , one can predict the R magnetic order on a $4b$ site for a given Mn order. This is reported in Table II. This description provides a simple way to distinguish two homometric configurations, knowing the order on the $4b$ sites. Experimentally, the intraplane Yb($4b$) coupling is AF while the interplane coupling is F. Therefore, the Mn order must be of Γ_4 type and Γ_2 can be discarded. This description also agrees with recent experiments^{30,32} in HoMnO_3 and can be easily extended to the rest of the RMnO_3 family.

C. Origin of the molecular field

The exchange energy between a Yb ion and its Mn first neighbors is classically written as a sum over Mn sites $\sum J \vec{S}_{\text{Mn}} \cdot \vec{S}_{\text{Yb}}$, where J is the isotropic first-neighbor exchange interaction. Each Yb atom (either on a $2a$ or $4b$ site) is at the

TABLE II. $R(4b)$ magnetic orders deduced for each configuration Γ_i of the Mn moments (i) by our analysis of the local magnetic environment using the sign of the A pairs and (ii) by the minimization of DM and dipolar energies. Both methods yield the same result.

| IR | A pair | $R(4b)$ coupling | |
|------------|--------------|------------------|------------|
| | | Intraplane | Interplane |
| Γ_1 | (+-) or (-+) | AF | AF |
| Γ_2 | (--) | F | F |
| Γ_3 | (-+) or (+-) | F | AF |
| Γ_4 | (++) or (--) | AF | F |

top of a pyramid with an equilateral triangular basis of Mn ions. Therefore, the exchange field induced at either Yb site cancels by symmetry for any of the Γ_{1-4} representations of the Mn magnetic order. Moreover, the classical exchange term cannot explain the perpendicular orientations of the R and Mn moments.

Experimentally, the exchange field is effectively zero at the Yb(2a) site (above 3.5 K), but it is not at the Yb(4b) site. So, in order to explain the $R(4b)$ magnetic order, we have to introduce an interaction which is not isotropic, i.e., which depends on \vec{r}_{ij} , the radius vector linking a $R(4b)$ to a Mn ion. This is the only way to obtain an out-of-plane effective field.

In the following we consider two interactions fulfilling this condition: the magnetic dipolar interaction and the Dzyaloshinskii-Moriya (DM) coupling between $R(4b)$ and Mn spins. The magnetic dipolar interaction is defined as

$$\mathcal{H}_{\text{dip}} = - \sum_{i,j} \vec{\sigma}_i \vec{B}_{ij}, \quad (4)$$

where \vec{B}_{ij} is the dipolar field induced by Mn moment j at $R(4b)$ site i and $\vec{\sigma}_i$ is the spin of the $R(4b)$ ion at site i .

The DM interaction between the Yb(4b) and the Mn moments is written as

$$\mathcal{H}_{\text{DM}} = \sum_{i,j} \vec{D}_{ij} \cdot (\vec{\sigma}_i \times \vec{S}_j). \quad (5)$$

According to the crystal symmetry and the rules defined by Moriya,³³ \vec{D}_{ij} is perpendicular to the mirror plane including both R and Mn sites, i.e., to the c axis, and defined as $\vec{D}_{ij} = \eta \vec{c} \times \vec{r}_{ij}$, where η is a spin-orbit coupling constant.

Although the dipolar and DM interactions are intrinsically different, they may be expressed in similar ways in terms of the A factors as follows:

$$\mathcal{H}_{\text{dip}} = \sum_i \sigma_i [(A_i r^z)^{\text{up}} + (A_i r^z)^{\text{down}}], \quad (6)$$

$$\mathcal{H}_{\text{DM}} = \eta \sum_i \sigma_i (A_i^{\text{up}} + A_i^{\text{down}}). \quad (7)$$

Minimizing the energy for these interactions should therefore lead to the same configurations as found in Sec. VI B. To confirm this, we have rewritten both interactions in terms of

a matrix J_{ij} (Ref. 29) such as $\mathcal{H} = \sum_{i,j} \vec{\sigma}_i J_{ij} \vec{S}_j$, where J_{ij} is expressed as

$$J_{ij}^{\text{DM}} = \begin{pmatrix} 0 & D_{ij}^z & -D_{ij}^y \\ -D_{ij}^z & 0 & D_{ij}^x \\ D_{ij}^y & -D_{ij}^x & 0 \end{pmatrix}, \quad (8)$$

$$J_{ij}^{\text{dip}} = \begin{pmatrix} r_{ij}^x r_{ij}^x & r_{ij}^x r_{ij}^y & r_{ij}^x r_{ij}^z \\ r_{ij}^y r_{ij}^x & r_{ij}^y r_{ij}^y & r_{ij}^y r_{ij}^z \\ r_{ij}^z r_{ij}^x & r_{ij}^z r_{ij}^y & r_{ij}^z r_{ij}^z \end{pmatrix} \frac{1}{r_{ij}^5}. \quad (9)$$

It is worth noting that the above matrices both have nondiagonal terms, which depend on the R -Mn pair considered. This is a necessary condition to ensure a nonzero interaction between Mn moments in ab plane and $R(4b)$ moments along the c axis.

We determined the stable Yb(4b) configuration for each IR of the Mn order. We find that both dipolar and DM interactions give the same result, in agreement with our analysis of the magnetic environment made above (see Table II). Namely, they stabilize the Γ_4 configuration of the Mn moments for the Yb(4b) order determined experimentally.

The analysis described here provides the conditions required for the magnetic interactions to yield the R and Mn magnetic orders observed experimentally. To go further, a quantitative calculation of the energy should be made. Our estimations made for the dipolar interaction show that it is too weak by 1 order of magnitude to fully account for the molecular-field constant $\lambda_{\text{Mn-Yb}} (= \lambda_1) = 2.1 \text{ T} \mu_B^{-1}$ found in Sec. VI A (Fig. 8). As for the DM interaction, estimation would require an evaluation of the relevant spin-orbit coupling constant.

We hope that this analysis will stimulate further theoretical work on the R -Mn interactions at the origin of the molecular field. This will allow one to understand the microscopic origin of the rare-earth magnetic order in the hexagonal RMnO₃ family.

VII. CONCLUSION

We have studied the magnetic order in YbMnO₃ and found a consistent description by combining Mössbauer and neutron probes. The temperature dependences of the Yb and Mn magnetic moments are well fitted in a molecular-field approach, showing that Yb(4b) moments order due to the Mn molecular field, whereas the Yb(2a) moments order at much lower temperature through Yb-Yb interactions.

We could determine the Mn magnetic structure and distinguish between two homometric configurations by considerations about the magnetic environment of each $R(4b)$ sites. In YbMnO₃, we found a Γ_4 configuration for Mn moments

associated with F stacking of AF Yb(4*b*) layers. This approach can be extended to the whole hexagonal RMnO₃ family. We propose possible mechanisms for the R-Mn interactions to be studied by further theories.

ACKNOWLEDGMENTS

We thank D. Colson for the sample preparation and F. Porcher and F. Bourée for the measurement on 3T2.

-
- ¹M. Fiebig, *J. Phys. D* **38**, R123 (2005).
²S. W. Cheong and M. Mostovoy, *Nature Mater.* **6**, 13 (2007).
³J. Park, J. G. Park, Gun Sang Jeon, Han-Yong Choi, Changhee Lee, W. Jo, R. Bewley, K. A. McEwen, and T. G. Perring, *Phys. Rev. B* **68**, 104426 (2003).
⁴S. Lee, A. Pirogov, M. Kang, K. H. Jang, M. Yonemura, T. Kamiyama, S.-W. Cheong, F. Gozzo, N. Shin, H. Kimura, Y. Noda, and J. G. Park, *Nature (London)* **451**, 805 (2008).
⁵A. Pimenov, T. Rudolf, F. Mayr, A. Loidl, A. A. Mukhin, and A. M. Balbashov, *Phys. Rev. B* **74**, 100403(R) (2006).
⁶H. Katsura, A. V. Balatsky, and N. Nagaosa, *Phys. Rev. Lett.* **98**, 027203 (2007).
⁷S. Petit, F. Moussa, M. Hennion, S. Pailhès, L. Pinsard-Gaudart, and A. Ivanov, *Phys. Rev. Lett.* **99**, 266604 (2007).
⁸T. Kimura, G. Lawes, T. Goto, Y. Tokura, and A. P. Ramirez, *Phys. Rev. B* **71**, 224425 (2005).
⁹Z. J. Huang, Y. Cao, Y. Y. Sun, Y. Y. Xue, and C. W. Chu, *Phys. Rev. B* **56**, 2623 (1997).
¹⁰T. Katsufuji, S. Mori, M. Masaki, Y. Moritomo, N. Yamamoto, and H. Takagi, *Phys. Rev. B* **64**, 104419 (2001).
¹¹E. F. Bertaut, *Phys. Lett.* **5**, 27 (1963).
¹²M. Fiebig, D. Frohlich, K. Kohn, S. Leute, T. Lottermoser, V. V. Pavlov, and R. V. Pisarev, *Phys. Rev. Lett.* **84**, 5620 (2000).
¹³J. A. Alonso, M. J. Martinez-Lope, M. T. Casais, and M. T. Fernandez-Diaz, *Inorg. Chem.* **39**, 917 (2000).
¹⁴J. Rodriguez-Carvajal, *Physica B* **192**, 55 (1993).
¹⁵M. Isobe, N. Kimizuka, M. Nakamura, and T. Mohri, *Acta Crystallogr., Sect. C: Cryst. Struct. Commun.* **47**, 423 (1991).
¹⁶B. B. Van Aken, A. Meetsma, and T. T. M. Palstra, *Acta Crystallogr., Sect. E: Struct. Rep. Online* **57**, i87 (2001).
¹⁷A. Muñoz, J. A. Alonso, M. J. Martinez-Lope, M. T. Casais, J. L. Martinez, and M. T. Fernandez-Diaz, *Phys. Rev. B* **62**, 9498 (2000).
¹⁸J. Fontcuberta, M. Gospodinov, and V. Skumryev, *J. Appl. Phys.* **103**, 07B722 (2008).
¹⁹H. Sugie, N. Iwata, and K. Kohn, *J. Phys. Soc. Jpn.* **71**, 1558 (2002).
²⁰P. Bonville, P. Imbert, G. Jéhanno, F. Gonzalez-Jimenez, and F. Hartmann-Boutron, *Phys. Rev. B* **30**, 3672 (1984).
²¹H. A. Salama, G. A. Stewart, D. H. Ryan, M. Elouneq-Jamroz, and A. V. J. Edge, *J. Phys.: Condens. Matter* **20**, 255213 (2008).
²²F. Gonzalez-Jimenez, P. Imbert, and F. Hartmann-Boutron, *Phys. Rev. B* **9**, 95 (1974).
²³A. Abragam and B. Bleaney, *Electron Paramagnetic Resonance of Transition Ions* (Clarendon, Oxford, 1969).
²⁴E. F. Bertaut, *C. R. Hebd. Seances Acad. Sci.* **252**, 76 (1961); *J. Phys. Radium* **22**, 321 (1961).
²⁵J. Rodriguez-Carvajal, <http://www.ill.eu/sites/fullprof/php/programsfa7c.html?pagina=GBasireps>
²⁶E. F. Bertaut, in *Magnetism*, edited by G. T. Rado and H. Shul (Academic, New York, 1963), Vol. 3, Chap. 4, p. 149.
²⁷D. P. Kozlenko, S. E. Kichanov, S. Lee, J. G. Park, and B. N. Savenko, *J. Phys.: Condens. Matter* **19**, 156228 (2007).
²⁸O. P. Vajk, M. Kenzelmann, J. W. Lynn, S. B. Kim, and S.-W. Cheong, *Phys. Rev. Lett.* **94**, 087601 (2005).
²⁹M. Fiebig, C. Degenhardt, and R. V. Pisarev, *Phys. Rev. Lett.* **88**, 027203 (2001).
³⁰A. Munoz, J. A. Alonso, M. J. Martinez-Lope, M. T. Casais, J. L. Martinez, and M. T. Fernandez-Diaz, *Chem. Mater.* **13**, 1497 (2001).
³¹P. J. Brown and T. Chatterji, *J. Phys.: Condens. Matter* **18**, 10085 (2006).
³²S. Nandi, A. Kreyssig, L. Tan, J. W. Kim, J. Q. Yan, J. C. Lang, D. Haskel, R. J. McQueeney, and A. I. Goldman, *Phys. Rev. Lett.* **100**, 217201 (2008).
³³T. Moriya, *Phys. Rev.* **120**, 91 (1960).